Mainz Microtron MAMI

Collaboration A2: "Tagged Photons"
Spokesperson: A. Thomas

Update Proposal for an Experiment

"Helicity dependence of single and double pion photoproduction processes and the GDH integral on the neutron"

Spokespersons for the Experiment:

P. Pedroni (INFN-Sezione di Pavia)

J. Annand (Department of Physics and Astronomy, University of Glasgow)

W. J. Briscoe (The George Washington University)

O. Jahn (Institut für Kernphysik, Universität Mainz)

J. Krimmer (Institut für Physik, Universität Mainz)

Abstract of Physics:

We propose to perform a precise measurement of the helicity dependence of the inclusive total absorption cross section on the deuteron and ^{3}He and of the quasi free meson photoproduction with neutral final states using the Crystall Ball/TAPS set-up, complemented by the threshold Cerenkov counter, together with the Mainz new frozen-spin polarised target and the circularly polarised MAMI-C photon beam. This measurement will give a much better insight into the GDH sum rule for the neutron and will allow an accurate investigation of the properties of the baryon resonances in the second and third region, and especially of the $D_{13}(1520)$, $D_{15}(1675)$ and $P_{33}(1600)$ states.

Abstract of Equipment:

We require a beam of tagged, circularly polarised photons incident on longitudinally polarised deuteron and ^{3}He targets. The 4π Crystal Ball photon spectrometer in combination with TAPS as a forward wall will be used. A threshold Cerenkov detector will be added for the on-line suppression of the background from electromagnetic events. The upgraded Glasgow tagging system will provide the tagged, polarised photon beam.

MAMI Specifications:

beam energy	450, 855 and 1558 MeV
beam current	< 20 nA
beam polarisation	polarised

Photon Beam Specifications:

tagged energy range	100 - 430 MeV; 400 - 800 MeV; 800 - 1480 MeV
photon beam polarisation	circularly polarized

Equipment Specifications:

detectors	Crystal Ball/TAPS, MWPC, PID, Cherenkov
target	frozen spin deuterated butanol (longitudinally polarised); longitudinally polarised ^{3}He gas at 6 bars

Beam Time Request :

set–up/tests with beam	100 hours
data taking	2100 hours
target repolarisation	300 hours

List of participating authors:

- **Institut für Physik, University of Basel, Switzerland**
  I. Jaegle, I. Keshelashvili, B. Krusche, Y. Maghrbi, F. Pheron, T. Rostomyan, D. Werthmüller

- **Institut für Experimentalphysik, University of Bochum, Germany**
  W. Meyer, G. Reicherz

- **Helmholtz–Institut für Strahlen- und Kernphysik, University of Bonn, Germany**
  R. Beck, A. Nikolaev

- **Massachusetts Institute of Technology , Cambridge, USA**
  A. Bernstein, W. Deconinck

- **JINR, Dubna, Russia**
  N. Borisov, A. Lazarev, A. Neganov, Yu.A. Usov

- **School of Physics, University of Edinburgh, UK**
  D. Branford, D.I. Glazier, T. Jude, M. Sikora, D.P. Watts

- **Petersburg Nuclear Physics Institute, Gatchina, Russia**
  V. Bekrenev, S. Kruglov, A. Koulbardis

- **Department of Physics and Astronomy, University of Glasgow, UK**
  J.R.M. Annand, D. Hamilton, D. Howdle, K. Livingston, J. Mancell, J.C. McGeorge, I.J.D. MacGregor, E.F. McNicoll, R.O. Owens, J. Robinson, G. Rosner

- **Department of Astronomy and Physics, Saint Mary's University Halifax, Canada**
  A.J. Sarty

- **Kent State University, Kent, USA**
  D.M. Manley

- **University of California, Los Angeles, USA**
  B.M.K. Nefkens, S. Prakhov, A. Starostin, I.M. Suarez

- **MAX-lab, University of Lund, Sweden**
  L. Isaksson

- **Institut für Kernphysik, University of Mainz, Germany**
  P. Aguar-Bartolome, H.J. Arends, S. Bender, A. Denig, E.J. Downie, N. Frömmgen, E. Heid, O. Jahn, H. Ortega, M. Ostrick, B.Oussena, P.B. Otte, S. Schumann, A. Thomas, M. Unverzagt

- **Institut für Physik, University of Mainz, D**
  J.Krimmer, W.Heil

- **University of Massachusetts, Amherst, USA**
  P.Martel, R.Miskimen

- **Institute for Nuclear Research, Moscow, Russia**
  G. Gurevic, R. Kondratiev, V. Lisin, A. Polonski

- **Lebedev Physical Institute, Moscow, Russia**
  S.N. Cherepnya, L.V. Fil kov, V.L. Kashevarov

- **INFN Sezione di Pavia, Pavia, Italy**
  A. Braghieri, A. Mushkarenkov, P. Pedroni

- **Department of Physics, University of Regina, Canada**
  G.M. Huber

- **Mount Allison University, Sackville, Canada**
  D. Hornidge

- **Tomsk Polytechnic University, Tomsk, Russia**
  A. Fix

- **Physikalisches Institut, University of Tübingen, Germany**
  P. Grabmayr, T. Hehl, D.G. Middleton
- **George Washington University, Washington, USA**
  W. Briscoe, T. Morrison, B.Oussena, B. Taddesse, M. Taragin
- **Catholic University, Washington, USA**
  D. Sober
- **Rudjer Boskovic Institute, Zagreb, Croatia**
  M. Korolija, D. Mekterovic, S. Micanovic, I. Supek

1 Introduction

Experiment A2-9/05 to measure the helicity dependence of single and double photoproduction processes and the GDH integral on the neutron has not requested beam time during the three years since it was approved with A-rating due to delays in the construction of the Mainz frozen-spin (deuterated) butanol target. The goals of the proposal remain, however, as timely as ever. In the present proposal we aim to update the scientific case and broaden the experimental scope, using a recently developed high-pressure, longitudinally-polarised ^{3}He target, which complements the properties of the frozen-spin target.

The nucleus of a polarised ^{3}He atom consists of two spin paired protons and a single unpaired neutron, making it appear approximately as a single polarised neutron. From calculations of the ^{3}He nuclear wavefunction one expects that the unpaired neutron carries about 90 % of the total ^{3}He spin [1]. Hence, the absence of free neutron targets make ^{3}He a valuable tool in the polarisation studies of the fundamental structure of the neutron.

The combination of two different polarised "nuclear" neutron targets and the capability of the experimental apparatus to identify cleanly different partial reaction channels will allow a precise quantitative evaluation of the corrections due to the bound nature of the polarised neutrons thus permitting an accurate determination of both the GDH integrand on the free neutron spanning a wide energy range and of the $\gamma n \to N\pi(\pi)$ channels.

In the present proposal, which represents a major revision of A2-9/05, we aim to achieve high-precision measurements of beam-helicity dependent observables:

- the total inclusive photoabsorption cross section on the deuteron in the photon energy range between 800 and 1450 MeV, where the statistical precision of the existing data is rather poor;

- the total inclusive photoabsorption cross section on ^{3}He in the photon energy range between 150 and 1450 MeV. This has not been measured previously. The ^{3}He and ^{2}H measurements will allow an accurate extraction of the value of the GDH integrand on the free neutron

- the $\gamma d \to np\pi^0(\pi^0)$ channels, between 200 and 1450 MeV, which were not feasible in previous GDH measurements. These data will allow an accurate investigation of the properties of the baryon resonances in the second and third region.

- the γ^3He $\to \pi^0 X$ channels in the Δ resonance region. These and the partial channel data on the deuteron will allow an accurate cross-check of the nuclear models employed to extract the free neutron information.

2 Physics motivations

2.1 The GDH sum rule on the neutron

The Gerasimov-Drell-Hearn (GDH) sum rule [2, 3] relates the anomalous magnetic moment (AMM) κ of a particle of spin S and mass M to the integral over the weighted helicity asymmetry of the total absorption cross section for circularly polarised photons on a longitudinally polarised target:

$$I_{GDH} = \int_{\nu_{th}}^{\infty} \frac{\sigma_p - \sigma_a}{\nu} \mathrm{d}\nu = 4\pi^2 \kappa^2 \frac{e^2}{M^2} S \tag{1}$$

where ν is the photon energy and σ_p (σ_a) denotes the total absorption cross section for parallel (antiparallel) orientation of photon and particle spins. The inelastic threshold ν_{th} corresponds to pion production (photodisintegration) threshold for a nucleonic (nuclear) target. This relation

gives a fundamental connection between ground state properties of a particle (rhs of eq. 1), and a moment of the entire excitation spectrum (lhs of eq.1), showing the equivalence of a non-vanishing κ with the internal dynamical structure of the considered particle. A measurement of the GDH integrand then represents a fundamental test of our knowledge of photo excitation of composite hadronic systems. Table 1 shows the magnetic moment (μ), the AMM and the GDH sum rule values for protons, neutrons, and ^{3}He nuclei.

For the nucleon case, an estimate of the GDH sum rule value can be performed using a combination of multipole analyses of the available single pion photoproduction data (mostly from unpolarised experiments) [4, 5] and phenomenological models of multipion and heavy meson photoproduction reactions [6, 7, 8] up to $E_\gamma \simeq 2$ GeV. Above this photon energy, the contribution can be estimated from Regge-type approaches [9].

In table 2 the current theoretical estimate of the GDH sum rule values is given for both the proton and the neutron. This estimates disagrees with the expected GDH sum rule value for the proton while it roughly reproduces the neutron GDH value. However, the (proton-neutron) difference has a different sign with respect to the GDH expectation.

It is also instructive to perform the isospin decomposition of eq. 1 for the nucleon case, which results in:

$$I^{p,n}_{GDH} = \frac{2\pi^2 e^2}{m^2}(\kappa_s \pm \kappa_v)^2 = I_{vv} + I_{ss} \pm I_{vs} \tag{2}$$

where the subscripts s, v denote the isovector and isoscalar parts of the anomalous magnetic moment, respectively. The dominance of the isovector component ($\kappa_v = 1.85\,\mu_N$) over the isoscalar one ($\kappa_s = -0.06\,\mu_N$) is responsible of the extreme sensitivity of the isovector-isoscalar term I_{vs} in the GDH integral to the different models. This interference term is responsible for the $(p - n)$ difference of the sum rule.

The first experimental check of the GDH sum rule for the proton was carried out jointly at the Mainz and Bonn tagged photon facilites, where I^p_{GDH} was measured in the photon energy range 200 MeV $< E_\gamma <$ 2.9 GeV [10, 11, 12, 13]. The combination of this result with the theoretical predictions for the unmeasured energy ranges (see table 3 [14]) supports the validity of the GDH sum rule for the proton at odds with the estimates given in table 2. The main reason of this discrepancy is the oscillating photon-energy dependence of the GDH integrand due to multipole contributions of alternating sign. Therefore, a reliable prediction requires a very high accuracy that has not been reached by any of the existing models.

This discrepancy emphasises the need of a precise test of the GDH sum rule for both the neutron and proton and for precise double polarisation data for all $\gamma N \to N\pi(\pi)$ channels, which give the dominant contribution to the GDH integral, in order to pin down the origin of the existing discrepancies.

For the neutron, the interpretation of the experimental data is more complicated than in the proton case due to the lack of free neutron targets necessitating the use of neutrons bound in ^{2}H or ^{3}He. Nuclear structure effects and final state interactions prevent the direct access to the free neutron cross sections and theoretical support is needed for their evaluation. A quantitative extraction of I^n_{GDH} is then necessarily model dependent.

Table 1: The magnetic moment μ (in units of the nuclear magneton μ_N), the AMM κ, and the GDH sum rule I_{GDH} in units of μb for protons, neutrons, deuterons and ^{3}He nuclei.

	p	n	d	^3He
μ	2.79	-1.91	0.86	-2.13
κ	1.79	-1.92	-0.14	-8.37
I_{GDH}	204	233	0.65	498

Table 2: Contributions of different partial reaction channels to the GDH sum rule. Predictions for $N\pi$ are from the SAID [4] and (within brackets) MAID [5] multipole analysis; estimates for $N\pi\pi$ are from [6]; estimates for $N\eta$ are from [5]; kaon channel contributions are from [7]; predictions for vector meson production are from [8]; Regge contributions are from [9].

	I_{GDH} proton	I_{GDH} neutron
$\gamma N \rightarrow N\pi$	172 [164]	147 [131]
$\gamma N \rightarrow N\pi\pi$	94	82
$\gamma N \rightarrow N\rho$	-8	-6
$\gamma N \rightarrow K\Lambda(\Sigma)$	-4	2
$\gamma N \rightarrow N\rho(\omega)$	0	2
Regge contribution ($E_\gamma > 2$ GeV)	-14	20
TOTAL	~ 239 [231]	~ 247 [231]
GDH sum rule	204	233

Table 3: The contribution (in μb) of various energy regions to the GDH integral I^p_{GDH} on the proton. The contribution for $E_\gamma < 0.2$ GeV is from the MAID [5] multipole analysis with an error estimated by a comparison with SAID [4]. The asymptotic contribution ($E_\gamma > 2.9$ GeV) is from [9] with an error estimated by a comparison with a similar approach [15].

E_γ (MeV)	I^p_{GDH}
≤ 0.2	-28.5 ± 2
0.2-0.8 (measured	226 ± 5 ± 12
0.8-2.9 (measured)	27.5 ± 2 ± 1.2
≥ 2.9	-14 ± 2
Total	211 $\pm 5 \pm 12$
GDH sum rule	204

The combined use of both "neutron-substitute" targets and the capability of the experimental apparatus to separate different partial reaction channels will play a crucial role in constraining the theoretical analyses and in establishing the validity of the models that will be used for this extraction. In particular, the comparison between the two different "free neutron" values that are extracted both from the deuteron and ^{3}He targets using different nuclear models will give a fundamental cross-check of the reliability of the extraction procedures.

While in the deuteron the proton and the neutron are essentially in s states of relative motion with aligned spins, ^{3}He is a system of two protons with spins paired off and an "active" unpaired neutron, again in relative s states. As a result we then find (see table 1) that

$$\mu_d \approx \mu_p + \mu_n \quad ; \quad \mu_{^3He} \approx \mu_n$$

so that the ^{3}He spin structure function is much closer to the free neutron than the deuteron. Therefore, it is expected that the measured GDH integrand function for ^{3}He above the pion photoproduction threshold will already be a good first approximation of the I^n_{GDH} value. A more quantitative evaluation can be performed by considering the part of the GDH integral for deuteron and ^{3}He above the pion production threshold. In a PWIA approach it can be

approximated as

$$\left[I^d_{GDH}\right]_{\nu>m_\pi} \sim p^d_p \cdot I^p_{GDH} + p^d_n \cdot I^n_{GDH} = 406\mu b,$$

$$\left[I^{3He}_{GDH}\right]_{\nu>m_\pi} \sim 2p^{3He}_p \cdot I^p_{GDH} + p^{3He}_n \cdot I^n_{GDH} = 197\mu b,$$

where p_p and p_n are the effective degrees of proton and neutron polarisation as evaluated by [16] when taking into account all nuclear wave function components ($p^d_p = p^d_n = 0.93$; $p^{3He}_p = -0.026$ $p^{3He}_n = 0.87$).

In this approach, Fermi motion and binding effects are neglected. However, as shown in [28], this simple approximation reproduces within a few %, the value of $\left[I^{3He}_{GDH}\right]_{\nu>m_\pi}$ evaluated with a complete nuclear model.

As outlined in section 5.1, the total photoabsorption cross section will be measured inclusively, i.e. without distinguishing between reaction on proton and neutron. Thus from the previous equations it can be clearly seen that the most accurate evaluation of I^n_{GDH} will come from ^{3}He, since the proton contribution to the measured helicity dependent yields, will be much smaller than in the deuteron case.

No polarised data exist for ^{3}He, while the helicity dependent total inclusive cross section on the deuteron has been measured from 200 MeV to 1.9 GeV at Mainz [23] and Bonn [25], as shown in fig. 1

The statistical precision of the data is fairly good at $E_\gamma \leq 800$ MeV [23], but it is still rather poor at the higher measured energies (see fig. 2). In this case there is a clear need of improvement in order to make a more stringent test of the different theoretical deuteron models.
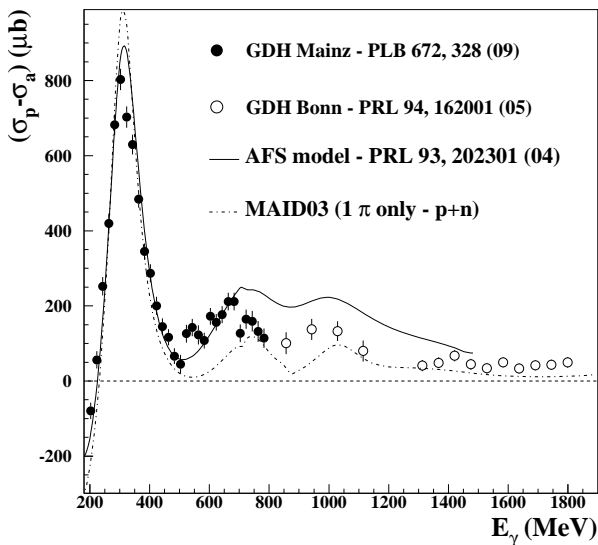

Figure 1: The helicity dependent total cross section on the deuteron obtained at Mainz [23] and Bonn [25].
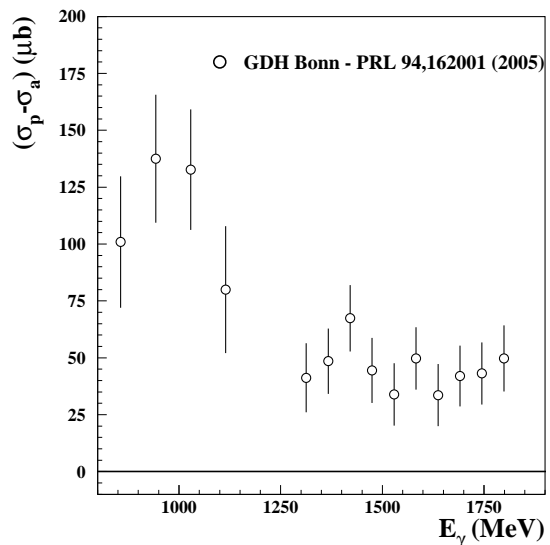
Figure 2: The helicity dependent total cross section on the deuteron obtained at Bonn.

In fig. 1, the experimental GDH deuteron results are also compared to a calculation by Arenhoevel, Fix and Schwamb (AFS) [27], which represent the most comprehensive microscopic nuclear deuteron model available up to now. In the same figure, the predictions of MAID [5] for the free $N\pi$ processes are also shown for an estimation of the role played by nuclear effects in the Δ resonance region. Discrepancies between the AFS deuteron model and the experimental results can be seen, especially in the upper part of the measured energy spectrum.

Improved theoretical descriptions of the γd interactions is clearly needed before any reliable evaluation of the free γn contribution can be performed.

2.2 The GDH sum rule on deuteron and ^{3}He

While the GDH sum rule gives similar results for the proton ($I^p_{GDH} = 204\,\mu b$) and the neutron ($I^n_{GDH} = 233\,\mu b$), a much smaller value is predicted for the deuteron ($I^d_{GDH} = 0.65\,\mu b$) due to the smallness of its anomalous magnetic moment ($\kappa_d = -0.143\,\mu_N$).

In AFS a strong anticorrelation between the photodisintegration process, which gives a large negative spin asymmetry immediately above break-up threshold ($E_\gamma \sim 2.2$ MeV), and the pion photoproduction reactions, which give a large positive contribution to I^d_{GDH} at $E_\gamma \gtrsim 140$ MeV, is predicted. Using this approach, the value $(I^d_{GDH})^{AFS} = 25\,\mu b$ was obtained, a factor of $\simeq 40$ higher than the expected I^d_{GDH} value.

Contrary to the deuteron case, ^{3}He photodisintegration processes have to show the same positive spin asymmetry as pion photoproduction reactions in order to fulfill the GDH constraint. Theoretical calculations of the GDH contribution below pion production threshold, evaluated using state-of-the-art three-body calculations [31, 32], predict a positive spin asymmetry but the estimated contributions exhibit a very strong dependence on the details of the current operators, which are still not well known. This feature is not present in the case of the unpolarised observables where, within each calculation, predictions based on different currrent operators agree (see, for instance, [24]).

In order to test the basic predictive ability of any model of deuteron or ^{3}He structure, precise experimental data are clearly required from photodisintegration threshold upwards.

The Mainz detection system is not suitable for accessing such low energies. However the collected data, both on the inclusive and on the partial reaction channels (see section 2.3), will allow a careful check of the deuteron and ^{3}He models beyond the π production region. Moreover, a direct measurement of both I^d_{GDH} and I^{3He}_{GDH} from the break-up threshold region up to around 60 MeV is planned at the newly upgraded HIγS facility of the TUNL laboratory (Durham NC, USA) [24].

Combined results from Mainz and HIγS will then provide a much deeper insight into both the full GDH sum rule for the deuteron and ^{3}He and the elementary mechanisms of the γd and γ^3He interactions.

2.3 Single and double π^0 photoproduction on the neutron

Apart from the contribution to the GDH sum rule, the helicity dependence of the $N\pi$ channels provides an important testing ground for multipole models. Up to now, estimates of the strength of different multipoles are mostly based on unpolarised single pion photoproduction data, the great majority of which were taken on the proton. However, as clearly demonstrated by the results from the GDH collaboration (see, for instance, [17]) the polarisation observables are a much better tool to disentangle the role of the different electromagnetic multipoles due to the change of sign of some contributions and to the presence of interference terms between different multipole amplitudes. For these reasons, the sensitivity to the smaller multipole amplitudes is greatly enhanced by the polarisation observables and a precise determination of the photon coupling to the different nucleon resonances is then possible.

The present proposal focuses on the measurement of the $n\pi^0$ channel, for which data are scarce even in the unpolarised case. These new data will enable a complete characterisation of the different isospin components of the multipole amplitudes and a better access to some resonant states as shown in Figures 3 and 4, where the MAID07 predictions for the helicity asymmetry

$$E = \frac{d\,\sigma_a - d\,\sigma_p}{d\,\sigma_a + d\,\sigma_p} = \frac{d\,\sigma_a - d\,\sigma_p}{2 \cdot d\,\sigma_{\text{unpolarised}}} \tag{3}$$

of the partial channels $\vec{\gamma}\vec{p} \to p\pi^0$ and $\vec{\gamma}\vec{n} \to n\pi^0$ are displayed as a function of the photon energy at $\theta_{cms} = 90°$ and $\theta_{cms} = 120°$ respectively. θ_{cms} represents the pion angle in the centre of mass system. The filled squares represent the standard MAID07 solution while the other curves represent solutions in which the coupling constant of a specific resonance state was set to zero. The difference between the standard and modified solutions provides a rough indication of the sensitivity of these observables to the different resonances.
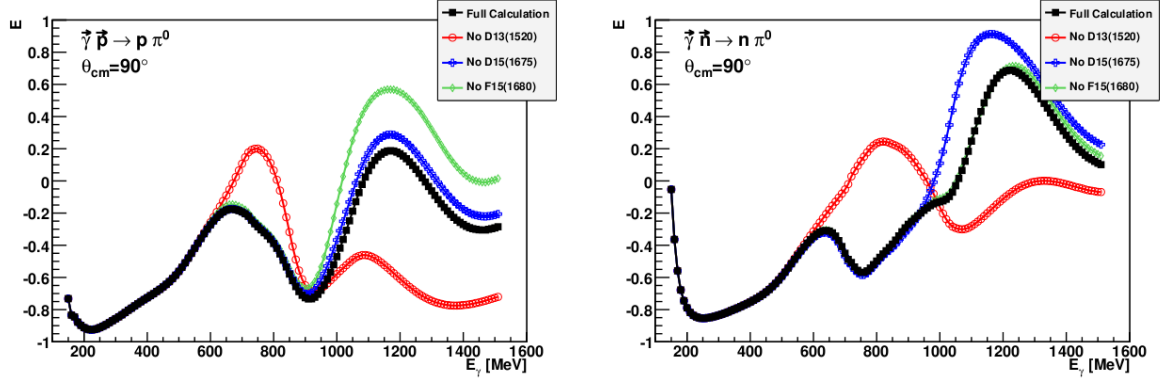
Figure 3: The sensitivity to different nucleon resonances of the helicity asymmetry E for the $\vec{\gamma}\vec{p} \to p\pi^0$ (left) and $\vec{\gamma}\vec{n} \to n\pi^0$ (right) reactions at $\theta_{cms} = 90°$ as predicted by the MAID07 model.
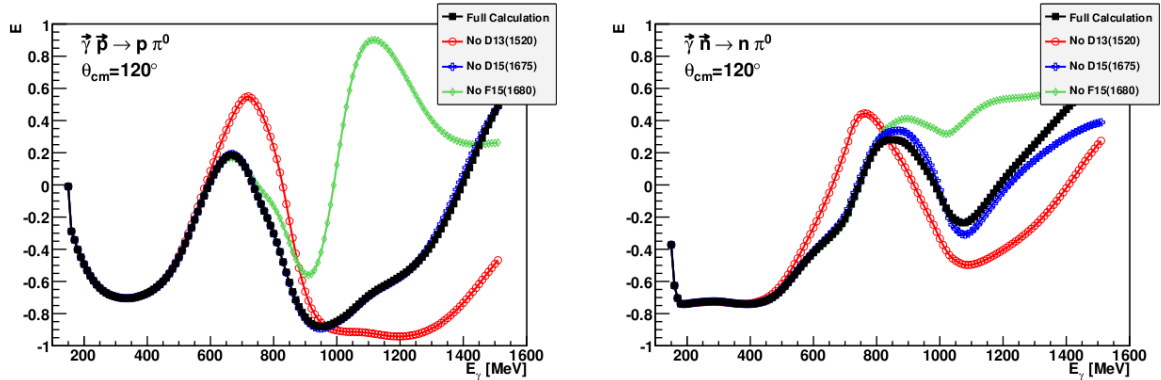

Figure 4: As in Figure 3 but for $\theta_{cms} = 120°$.

While the sensitivity to the $D_{13}(1520)$ resonance is similar for both channels, the model predicts a strong isospin dependence of the helicity amplitudes associated with the $D_{15}(1675)$ and $F_{15}(1680)$ states.

Table 4: Helicity amplitudes $A_{1/2}$ and $A_{3/2}$ for the $D_{13}(1520)$, $D_{15}(1675)$ and $F_{15}(1680)$ resonances.

	$D_{13}(1520)$		$D_{15}(1675)$		$F_{15}(1680)$	
	proton	neutron	proton	neutron	proton	neutron
$A_{1/2}$	$[-38, -7]$	$[-67, -48]$	$[15, 34]$	$[-57, -33]$	$[-17, -9]$	$[17, 32]$
$A_{3/2}$	$[143, 168]$	$[-158, -124]$	$[10, 24]$	$[-77, -51]$	$[115, 145]$	$[-40, -23]$

Table 4 shows the range of values for the helicity amplitudes $A_{1/2}$ and $A_{3/2}$ for these resonances, as predicted by the different $\gamma N \to N\pi$ partial wave analyses listed in the Review of
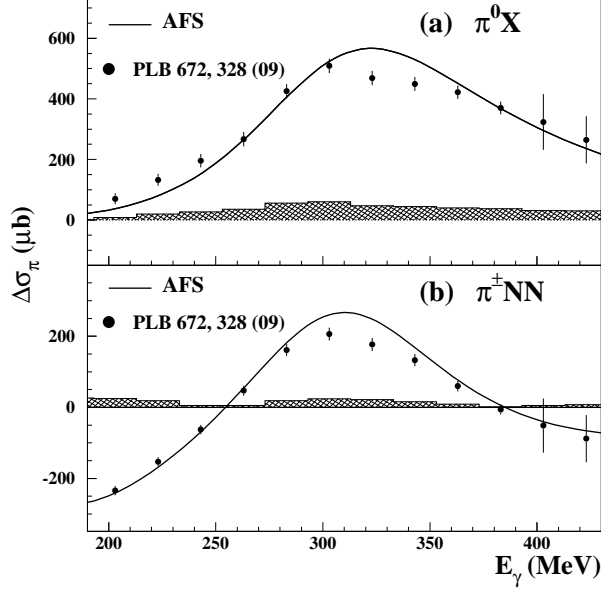
Figure 5: The helicity dependent total cross section for the semi-exclusive channels (a) $\gamma d \rightarrow \pi^0 X (X = pn \text{ or } d)$ and (b) $\gamma d \rightarrow \pi^{\pm} NN$ from [23] are compared to the AFS model predictions in the Δ-resonance region. The hatched bands show the systematic uncertainties.

Particle Physics [18]. The systematic differences between the analyses, caused by using different parametrisation schemes, are indicative of the true uncertainties in the determination of these quantities As can be clearly seen from this table, our knowledge of the helicity amplitudes is still quite poor.

This statement is supported by the recent publication [23] of the first helicity dependent total cross section data for semi-inclusive $\gamma d \rightarrow \pi^0 X$ and $\gamma d \rightarrow \pi^{\pm} NN$ in the Δ resonance region. These data are shown in fig. 5, compared with the prediction of the AFS model.

The AFS model overestimates both partial channels around the Δ resonance peak region and at lower energies underestimates the $\pi^0 X$ channel (Fig. 5 a), for which the nuclear effects are more important than in the $\pi^{\pm} NN$ case. As shown for instance in Ref. [27], the values of the helicity dependent cross section $(\sigma_p - \sigma_a)$ in the Δ resonance region for the $\pi^0 pn$ channel are reduced by about 40% when FSI are added to the pure quasi-free mechanisms.

These facts strongly motivate further theoretical and experimental research in the field. In particular, even in the Δ resonance region, further differential helicity dependent data, especially on the reaction channels having a π^0 in the final state, are needed to clarify the situation.

This partial channel study will be performed using the deuterated butanol target, due to the higher luminosity that can be reached. However, in the Δ resonance region, where the cross section is higher, reasonable precision will be obtainable with the ^{3}He gas target in this region. Since nuclear effects are most important, the comparison will further constrain the nuclear models that are needed for evaluation of the free-neutron contribution.

As an example, in Fig. 6 the measured total cross sections on ^{2}H and ^{3}He from [29] are compared with the corresponding πX predictions from [27] and [30]. Taking into account that the theoretical curves do not include the contribution given by the photodisintegration channels, it is clear that our present theoretical descripion on the single π photoproduction on the light nuclei is not satisfactory even in the unpolarised case.

The $n\pi^0\pi^0$ channel will provide additional and complementary information on the different baryon resonances. Its sensitivity to the resonant states is enhanced with respect to the other $\gamma n \rightarrow N\pi\pi$ channels since the intermediate $\Delta\pi$ Born terms dominating the channels with
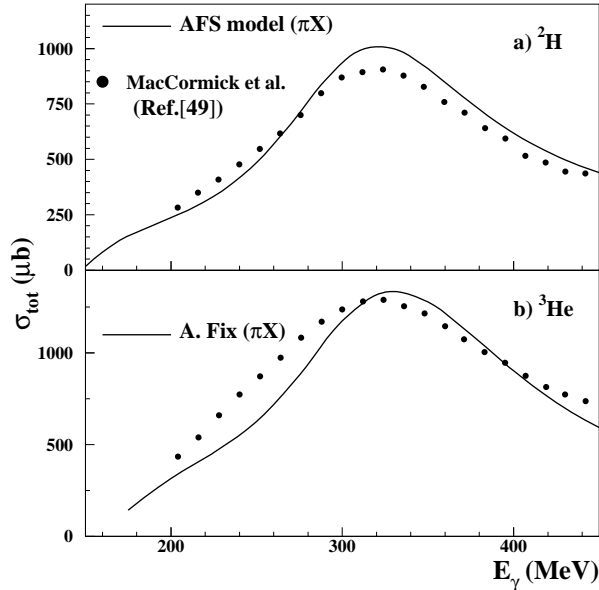
Figure 6: The unpolarised total cross sections for (a) deuteron and (b) ^{3}He from ref.[29] compared to the πX predictions of (a) AFS [27] and (b) A.Fix [30] in the Δ-resonance region.

charged pions are strongly suppressed and, due to isospin conservation, no intermediate ρ contribution is possible.

This reaction will be particularly useful for those states having very large branching ratios to $N\pi\pi$ channels and small branching ratios to $N\pi$ channels. This is the case for the $P_{33}(1600)$ resonance, that has an estimated $N\pi$ ratio between 10% and 25% and an estimated $N\pi\pi$ ratio between 75% and 90% [18].

The double polarisation data obtained by the GDH collaboration for the $\gamma p \to N\pi\pi$ channels up to 800 MeV [19, 20, 21] were described only semi quantitatively by existing models, due to the complicated nature of the underlying mechanisms. In this case, new data on both the proton and the neutron are essential to solve the existing discrepancies and to greatly improve our very poor knowledge of the $N\pi\pi$ reactions. The partial-wave formalism developed by the Bonn-Gatchina group [22] represents a valuable tool for this type of analysis.

3 Experimental setup

General details for most of the experimental setup used for this experiment, such as the photon tagging system, the butanol polarised target system and the Crystal Ball / TAPS detector systems are described in appendix A.

In the following only the particular devices required by the proposed measurements will be described.

4 The Polarized ^{3}He target

Polarized ^{3}He gas has been used for many years as a substitute for a polarized neutron target in electron scattering experiments at MAMI (see [33, 34] and references therein). The expertise from these experiments has been used to adapt the existing target technologies for use in conjunction with a tagged photon beam and a 4π detector.

4.1 Target cell

The Crystall Ball (CB) detector puts geometric constraints on the space available for any target system.

In order to fit inside the inner part of the CB detector and to reach a useful experimental luminosity, the target cells are cylindrical with an outer diameter of 6 cm and a total length of 20 cm. Under these conditions, with a gas pressure of 6 bar, the number of target atoms is $N_T \sim 3 \cdot 10^{21}/cm^2$. Although the ^{3}He gas target has a relatively low density, it is pure, so that the fraction of polarised neutrons is greater than in the deuterated butanol case.

The target cell is made from quartz glass with entry and exit windows for the photon beam (see Fig. 7). Two different window materials, i) aluminised mylar glued to aclar (a resin providing a very high moisture barrier) and ii) beryllium, are currently being investigated. These materials provide the necessary gas tightness and were also found to give acceptably long relaxation time of the gas polarization (see 4.2). In both cases, each window will be 150 μm thick.
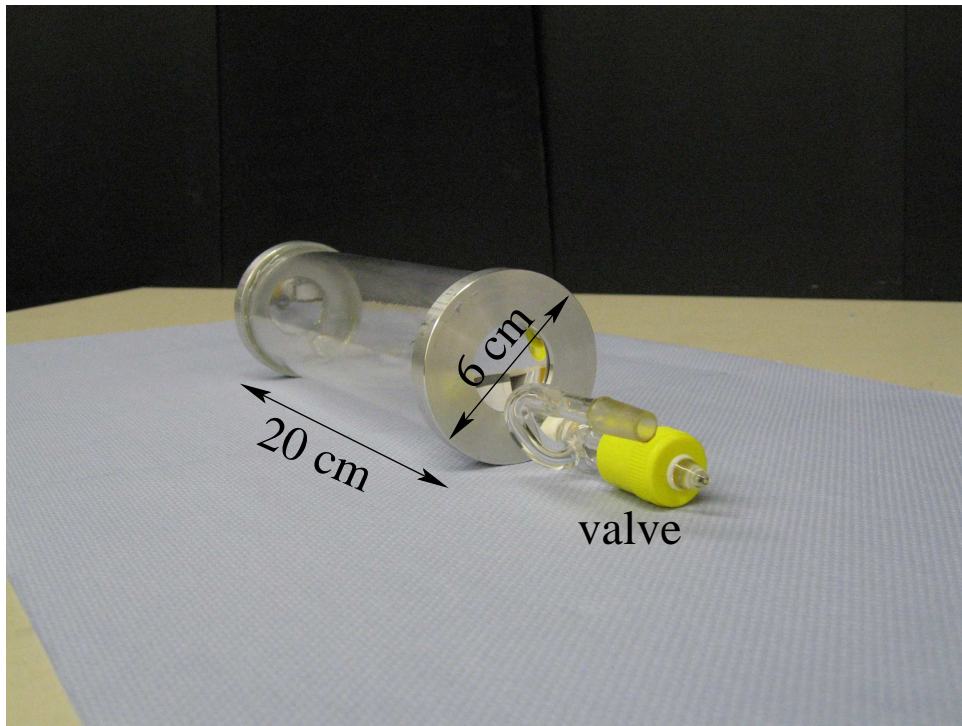

Figure 7: Target cell for use in the photon beam.

The window foils are glued, using Araldite 2011, to Al caps (Fig.7) which provide some mechanical support to hold the 6 bar pressure. A glass valve [1] is provided to ease filling and venting of the cells.

After filling at the polarizer in the Institute of Physics, the target cell is brought to the A2 experimental area at MAMI and inserted inside the CB detector, where the polarisation alignment is maintained by a solenoid inside a region with a very low magnetic fied gradient (see 4.3) This mode of operation has been employed successfully in a measurement of $G_{e,n}$ via the ^{3}He$(e, e'n)$ reaction [40] in the A1 spectrometer hall at Mainz.

---

[1]Young POR 3/glass

4.2 Polarization and relaxation

Gasesous ^{3}He is polarized via the method of Metastability Exchange Optical Pumping (MEOP) [35, 36]. The metastable 2^3S_1 state is reached via a gas discharge at pressures of 0.8-1.0 mb and can then be optically pumped by circularly polarized laser light at 1083 nm. The nuclear polarization of the 2^3S_1 state is transferred to unpolarized ground state atoms via collisions. After polarization buildup the gas is compressed to the desired pressure of about 6 bar by a nonmagnetic piston where less than 2% of the polarization is lost [37]. 2 bar·l of ^{3}He can be polarised per hour to values $> 70\%$ [38, 39].

Different processes contribute to the total relaxation time T_1^{total}:

$$\frac{1}{T_1^{total}} = \frac{1}{T_1^{grad}} + \frac{1}{T_1^{dipole}} + \frac{1}{T_1^{wall}}$$

Provided that the relative field gradient $((dB/dr)/B_0)$ is smaller than $5\cdot10^{-4}$ cm^{-1} the partial relaxation time T_1^{grad} is larger than 1000 hours at a pressure of 5 bar [42]. At higher pressures p the total relaxation time is limited due to dipole dipole interaction between ^{3}He atoms. ($T_1^{dipole} = 817$ h$/p$ [bar] [43]). The wall relaxation, i.e. the loss of polarization due to the collisions of ^{3}He atoms with the walls of the target container is reduced by caesium coating and an appropriate degaussing procedure.

From the experience gained with the previous A1 experiments, a wall relaxation time T_1^{wall} of about 40 hours is expected for these cells after degaussing and caesium coating. In July 2008, during the last A1 experiment, initial polarisation values greater than 70% were obtained. With a total relaxation time of 30-40 hours and a target cell exchange twice per day, this resulted in a mean polarization of 55-60% [41].

4.3 Target Setup

In Fig. 8 a side view of the target setup is given. During the experiment the target cell is located in the middle of a solenoid (length = 80 cm, diameter = 8 cm, 1500 turns) inside the Crystal Ball (CB) detector. The measured relative field gradient along the axis $(dB_z/dz)/B_0$ is smaller than $5 \cdot 10^{-4}$cm^{-1} [44].

A pair of Helmhotz coils (diameter = 1.6 m) is located upstream of CB; this system comprises the additional coils necessary for polarimetry. The transfer of the target cell between the position in the Helmholtz coils and the position inside CB during the normal data-taking phases is performed via a nonmagnetic transport system[2].

Polarisation monitoring and measurement are accomplished by two means. A relative measure of the polarisation is done via a NMR technique. Applying a static magnetic pulse perpendicular to the holding field rotates the magnetization out of the horizontal plane by an angle $\alpha \approx 2°$. The signal amplitude (free induction decay monitored via pickup coils) yields only a relative measure of the polarisation, but allows one to monitor the decay of polarisation (relaxation) with high precision. The relative loss of polarisation due to this technique is 0.02% per measurement.

The measurement of the magnetic field produced by a dense sample of polarized gas is used to determine the absolute ^{3}He polarisation [45]. As the field produced by the cell B_{cell} is on the order 1 mG, which is more than an order of magnitude smaller than the holding field B_0=9 G, the total field is measured before and after a 180° spin flip via a fluxgate magnetometer[3]. The difference $\Delta B = (B_0 + B_{cell}) - (B_0 - B_{cell}) = 2 \cdot B_{cell}$ is independent of B_0 (see Fig. 9 for the setup

---

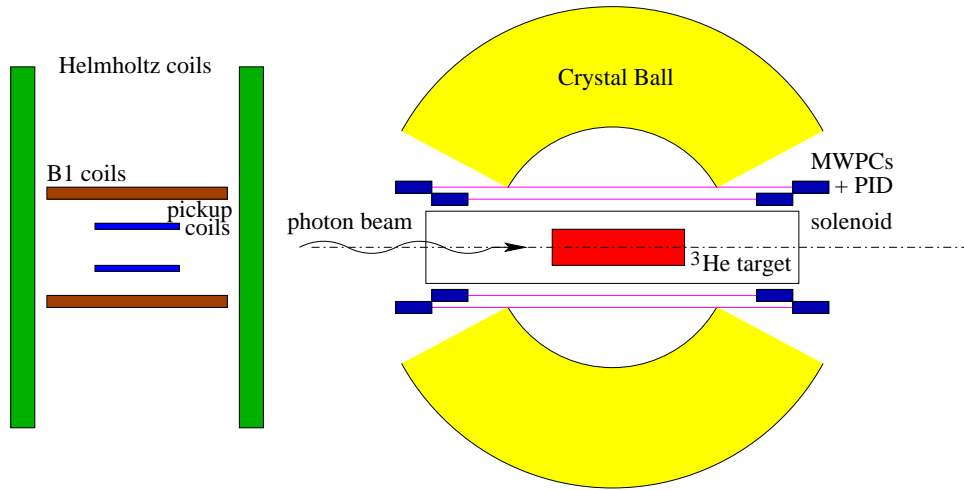[2]igus DryLin Zahnriemenachse

[3]Bartington MAG03-IEHV 1000

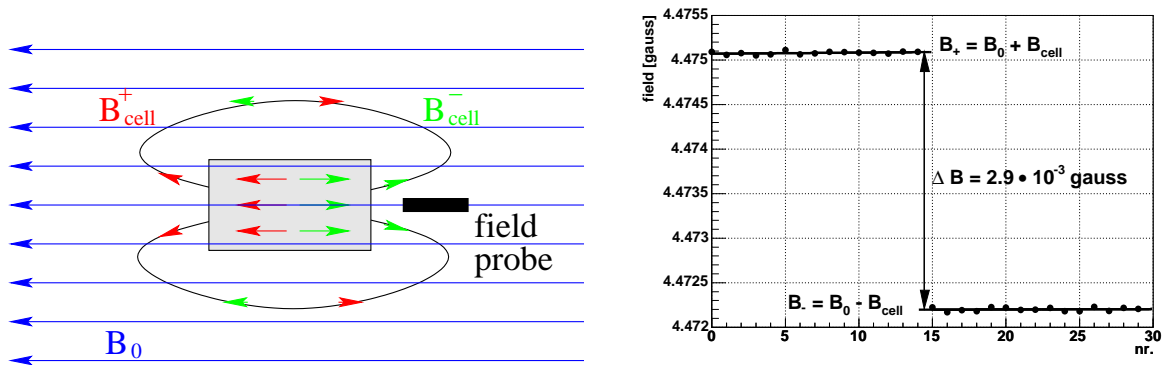Figure 8: Side view of the experimental setup

Figure 9: Left: Sketch of the setup for AFP measurement. Right: Magnetic field before and after the 180° spin flip. The difference ΔB is directly proportional to the ^{3}He polarisation.

and a measurement of ΔB). The reversal of the magnetization with respect to the guiding field is done via adiabatic fast passage (AFP). After calibration, the absolute polarisation is determined with a systematic uncertainty of less than 4%.

4.4 Results from test measurements

A feasability test has been performed to study the ratio of nuclear scattering events produced on the target cell windows to that produced on the gas [44].

A quartz glass cell having two 50 μm thick kapton windows was inserted into the Crystal Ball detector and filled with ^{4}He gas at 6 bars. It was found that that the number of hadronic events produced by the entry windows of the target cells was about 90% of the number of events produced by the gas inside the cell.

Given this result, we evaluate that in the case of ^{3}He gas and two 150 μm thick berillyum windows, the worst case among the materials under test, the previous ratio becomes 4:1.

In a further test measurement, the transfer of a cell filled with polarized gas from the field of the Helmholtz coils to the solenoid inside CB has been studied. It turned out that the relative polarization losses for the transfer can be kept below 1%.

4.5 The hadron detector

In addition to the standard CB and TAPS setup, for the reasons that will be detailed in sec. 5.1, the measurement of the total inclusive cross section requires a threshold gas Cherenkov detector to suppress the events from electromagnetic (e.m.) reactions inside the target. This detector will be installed between the CB frame and the TAPS detector to cover the angular polar region from $0°$ to $18°$, where practically all e.m. events take place.
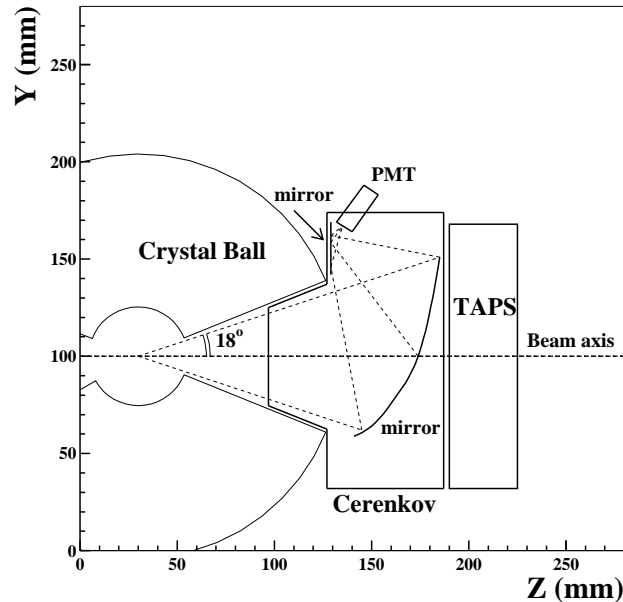

Figure 10: Schematic side view of the experimental setup including the Cherenkov detector.

The aim of this apparatus is the detection of $e^{\pm}$ but a complete insensitivity to hadronic reaction products. Since the lightest generated hadron is the pion ($m \simeq 140$ MeV) and the highest possible beam energy is about 1.5 GeV, it follows that the maximum possible kinetic energy for the pion will be close to about 1.4 GeV.

Cherenkov light is emitted by particles having $\beta > 1/n$ (where n is the refractive index of the medium); it follows that a medium having $n < 1.004$ is needed in our case. A suitable gas is then C_4F_8 ($n = 1.0013$), which has also a good transparency for light in the UV range, where a large part of the Cherenkov radiation is emitted.

A schematic drawing of the complete detector geometry is shown in figure 10. The gas Cherenkov detector is shaped to fit snugly inside the backward aperture of the CB This additional device will have a composite shape due to the need to use a part of the space inside the downstream part of the CB tunnel region, with a total volume of $\sim 1.3\text{m}^3$ and a light emission length along the z(beam)-axis (L_{rad}) of about 70 cm.

The gas volume is be enclosed in a light and gas-tight aluminium casing containing 100 μm entrance and exit windows, each consisting of two thin mylar and tedlar foils. The Cherenkov light is focused by an ellipsoidal mirror onto a 5 inch photomultiplier tube (PMT). Mechanical construction is similar to the thershold Cherenkov used for previous GDH measurements [47]. The PMT and mirror have been reused for the present detector. The mirror, made out of perspex, has a central hole with a diameter of 5 cm for the passage of the photon beam. The hole is covered by a highly reflecting mylar foil in order to avoid losses of Cherenkov light. Full technical details can be found in [46].

A computer simulation, which takes into account light propagation, reflection and the photocathode conversion probability predicts an efficiency of 100%. From a dedicated test measurement performed on the A2 beamline an efficiency of $99.95 \pm 0.01\%$ was measured with a detector only partially (around 80%) filled with C_4F_8, in good agreement with the expectations.

5 Experimental method

5.1 Total inclusive cross section measurement

For the considered photon energy range, photoabsorption processes lead to many different multiparticle final states which may be difficult to identify individually and have quite different acceptances and detection efficiencies. To avoid large, systematic uncertainties arising from unobserved final states, the total photoabsorption cross section has to be measured inclusively, as was done by the GDH collaboration both at Mainz and Bonn.

For this reason, it is necessary to observe at least one reaction product of any of the possible hadronic final states with as high as possible acceptance in terms of solid angle and efficiency. Any loss of events due to limited acceptance must be estimated using models and obviously the loss of events must be minimised to minimise the model dependence of results The identification of individual processes is not necessary; what is needed is the reliable detection of charged particles and a high efficiency for the neutral decay modes of hadrons. The CB-TAPS detector, a solid angle covering of 97% of 4π and a detection efficiency $\gtrsim 99\%$ for both charged hadrons and photons from neutral meson decays, meets these requirements.

The trigger condition required for a total cross section measurement is just the detection of one or more charged or neutral hadrons in the CB or TAPS. In figure 11 the simulated detection efficiency for all $N\pi$ channels is shown, for this condition, as a function of the pion angle in the center of mass system at $E_\gamma = 1.0$ GeV. Neutron signals were not used for this evaluation; Charged hadrons or photons with an energy release of greater than 40 MeV were taken into account, but neutron were not considered.

These single pion channels represent the worst case for the detector acceptance and when at least one additional pion is emitted in the final state, the efficiency is very close to 100% over the full angular range.

For the $n\pi^+$ channel, the most unfavorable case, the unmeasured part of the cross section represents, in the unpolarised case, only $\simeq 2\%$ of the total cross section for this particular channel and $\simeq 0.4\%$ of the total inclusive cross section for the deuteron.

In order to minimize the errors associated with the extrapolation into regions outside the detector acceptance the ability of the detector to identify particular charged and neutral reaction channels will be used both for the experimental evaluation of the total cross section correction terms and for a cross-check of the analysis procedure. The overall systematic error of the measurements will be similar or better than the previous GDH experiment ($\simeq$ a few % of σ_{tot}).

Since very loose trigger condition are necessary, it is vital to suppress e.m. interactions (pair production and Compton scattering) of the photon beam with the target, which have cross sections several orders of magnitude grater than the hadronic processes.

This background, which is overwhelmingly concentrated in the forward direction than the hadronic events, has to be suppressed on-line by about 3 orders of magnitudes so that it does not pollute hadronic processes significantly.

This rejection will be performed with the threshold Cherenkov counter located in the forward polar angular region that has been previously described in section 4.5.

A feasibility test of a total inclusive measurement has recently been performed with an unpolarised liquid hydrogen target. During this first test, trigger conditions similar to the ones that will be implemented for the total cross section measurement (presence of at least on particle in
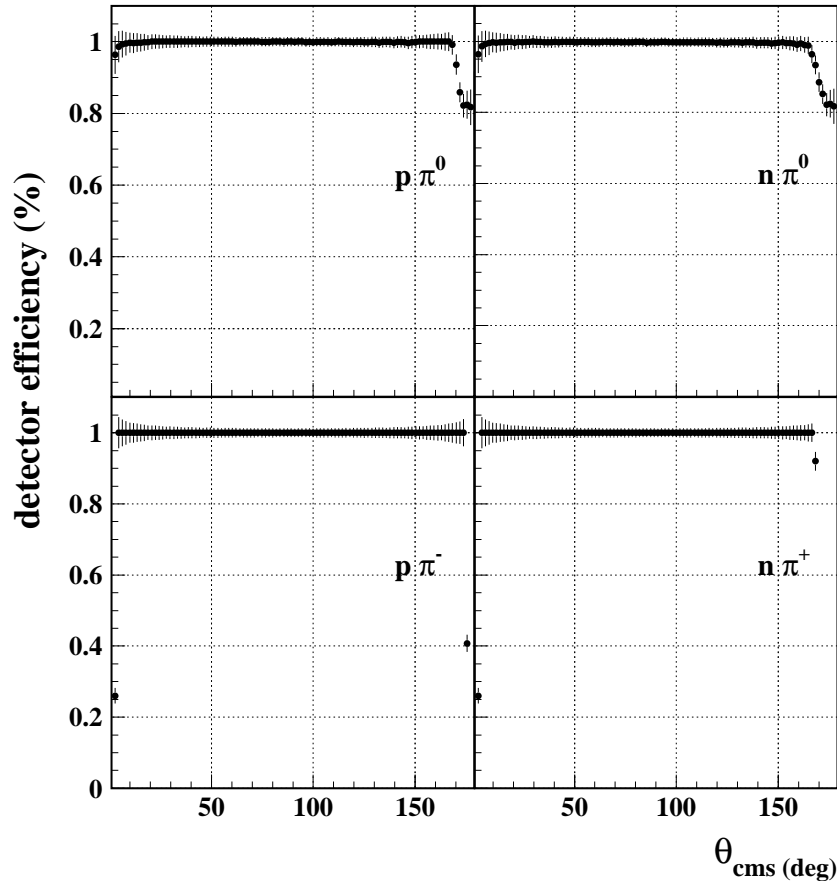
Figure 11: Simulated detection efficiency for all $N\pi$ channels at E_γ=1 GeV as a function of the π angle in the center-of-mass system.

the CB and at least 2 particles inside TAPS) were used. The online Cherenkov veto conditions eliminated around 10% of the CB raw triggers and around 75% of the TAPS raw triggers.

In fig. 12 the results obtained from the first preliminary, offline analyses are shown and compared to the existing data. These results were not corrected for events falling outside the detector acceptance or for trigger inefficiencies.

The small underestimations up to around 500 MeV are then mainly due to single charged particle events hitting but not triggering TAPS (for instance π^+ from the $n\pi^+$ channel or a charged pion from the $p\pi^+\pi^-$ channel close to threshold, when only one of the charged pions has enough energy to reach TAPS.

Above 600 MeV, our data are in agreement with previous data. In this energy region multi-hadron processes dominate and the probability that something makes a trigger becomes very high.

In the upper part of the measured photon energy interval, our points slightly overestimate the previous data. This is due to an approximate evaluation of the empty target contribution, which is quite large in the considered region.

On the basis of this preliminary analysis (Fig.12) we are confident that extrapolation corrections to the total cross section will be small, even in the polarised case. Corrections will be further reduced when a more open TAPS trigger is implemented.
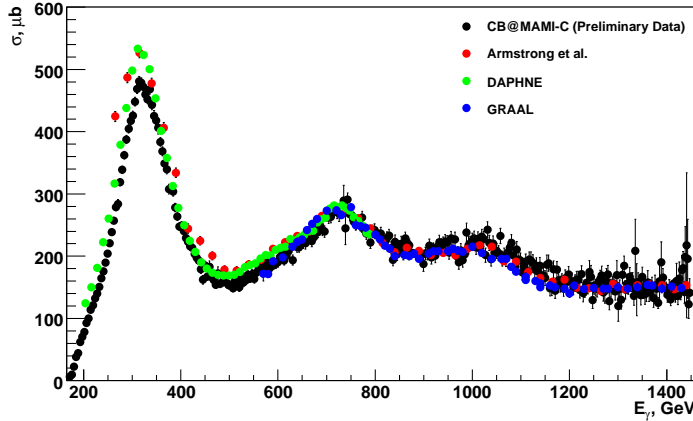
Figure 12: The preliminary data obtained on the unpolarised total inclusive cross section on hydrogen (black circles) are compared to the existing published data of ref. [50] (red circles); ref. [29] (green circles) and ref. [51] (blue circles). Only statistical errors are shown.

5.2 Measurement of single and double photoproduction channels

The use of the Cherenkov detector will be very useful also for the partial channel measurements since it will extend the accessible angular range into the forward polar region ($\theta < 20°$), where in general the strongest variations in cross sections and asymmetries can be found.

In this case the trigger conditions will be a combination of the standard cluster triggers requiring cluster multiplicities of ≥ 2, since the channel identification requires the detection of all particles (neutron and γs from π^0 decay) in final state.

In figure 13, the θ_{cms} angular region available for the coincident detection of all final state particles is shown for the $n\pi^0$ reaction as a function of E_γ. Neutron detection was assumed to be effective for kinetic energies ≥ 50 MeV Starting from $E_\gamma \simeq 350$ MeV, most of the angular region can be covered by the present apparatus.

As demonstrated by previous DAPHNE [48] and TAPS [49] data, final state interactions and nuclear effects do not play a significant role for the quasi-free processes far from the π production threshold and the extraction of the free neutron information can be performed in a quite reliable way.

For $n\pi^0\pi^0$ simulations show that at $E_\gamma \simeq 600$ MeV almost 80% of the total phase space region can be accessed; this value rises to about 90% at $E_\gamma \simeq 1$ GeV to reach a maximum of about 95% at $E_\gamma \simeq 1.4$ GeV.

Due to the good capabilities for charged particle identification, the possibility of investigation of other quasi-free partial channels ($p\pi^-\pi^0$, $n\pi^+\pi^-$, ...) will be also explored.

6 Beam time estimate

The count rate estimate is based on the usual formula:

$$N_{tot} = (N_\gamma \cdot \Delta t) \cdot (f \cdot \cdot dN_T) \cdot \epsilon_{det} \cdot \langle \sigma_{unpol} \rangle \tag{4}$$

where:

- N_{tot} is the total number of polarised events;

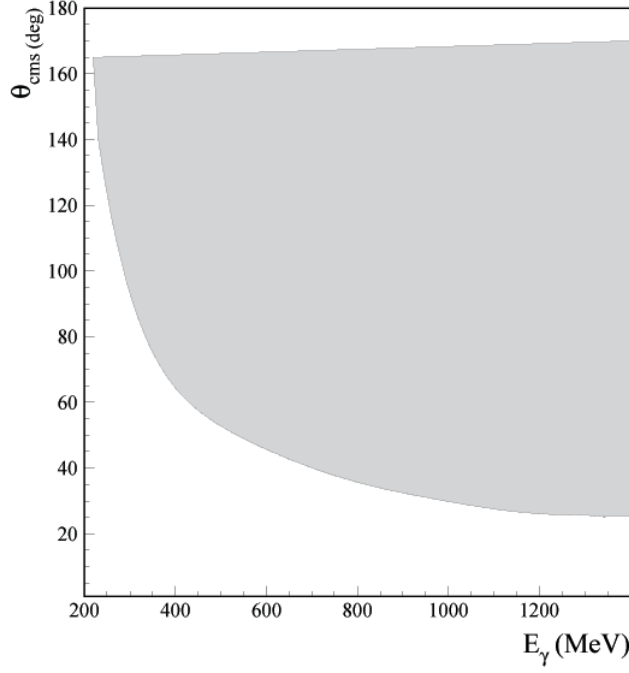- N_γ is the photon flux for a given energy bin;

Figure 13: Covered kinematical region in (E_γ, θ_{cms}) for the $n\pi^0$ reaction.

- Δt is the data taking (exposure) time;

- f is the target dilution factor;

- f is the target filling factor;

- N_T is the number of target neutrons;

- ϵ_{det} is the detection and reconstruction efficiency;

- $\langle \sigma_{unpol} \rangle$ is the averaged cross section within the selected photon energy range.

The connection between the polarised cross section difference $\Delta\sigma$ and the helicity asymmetry E is given as:

$$E = \frac{\sigma_p - \sigma_a}{\sigma_p + \sigma_a} \quad ; \quad \Delta\sigma = \sigma_p - \sigma_a = E * 2 * \sigma_{unpol} \tag{5}$$

which is used for the count rate estimate in each photon energy bin.

For each bin, the total number of measured events N_p and N_a for the two total helicity states is given by:

$$N_p = N_0(1 + PE + B + C) \tag{6}$$
$$N_a = N_0(1 - PE + B + C) \tag{7}$$

where

- N_0 is the number of unpolarised events

- $P = \langle P_\gamma \rangle \cdot \langle P_T \rangle$ is the product of the average values of beam and target polarisation

- B is the background contribution due to unpolarised nucleons ($1/f = 1 + B$)

- C is the background contribution due to the target cell materials

The combined effects of $P < 1$ and of the B and C background terms lead to a dilution of the measured asymmetry E_{meas}

$$E = \frac{\eta}{P} E_{meas} = \frac{\eta}{P} \cdot \frac{N_p - N_a}{N_p + N_a} \tag{8}$$

with $\eta = 1 + B + C$. The statistical uncertainty of E is then given by:

$$\delta E_{stat}^2 = \frac{1}{P^2} \frac{\eta}{2N_0} \left[1 - \left(\frac{PE}{\eta} \right)^2 \right] \tag{9}$$

and (neglecting the small quadratic correction) the total number of events N_{tot} needed for both helicities state results:

$$N_{tot} = 2N_0 = \frac{\eta}{P^2} \cdot \frac{1}{\delta E_{stat}^2} \tag{10}$$

Combining eqs. 4 and 10, the estimated beam time is

$$\Delta t = \frac{\eta}{P^2} \frac{1}{\delta E_{stat}^2} [I_\gamma \cdot (f \cdot N_T) \cdot \epsilon_{det} \cdot \langle \sigma_{unpol} \rangle]^{-1} \tag{11}$$

In the following separate beam time estimates will be given for deuterated butanol and ^{3}He . In both cases, as described above, an average degree $\langle P_\gamma \rangle = 0.6$ will be used for the photon polarisation

6.1   Deuterated butanol target

The parameters entering the count rate estimate are:

- Incoming electron beam energy: $E_0 = 450$, 855 and 1500 MeV;

- Tagged photon energy range: upper half of the photon energy range;

- Photon flux $I_\gamma = 7 \cdot 10^5 / (sec \cdot 20$ MeV); this corresponds to the maximum estimated photon flux value that does not cause heating (and then depolarisation effects) in the deuterated butanol.

- polarised target nucleon density is $f \cdot d \cdot N_T = 9.1 \cdot 10^{23}$ (cm^{-2}) for a 2 cm length;

- the target dilution factor amounts to $f = 20/84 = 0.24$, due to carbon and oxygen nuclei. This gives $B = 3.2$.

- the background due to the target cell materials is $C = 4$, as derived from the previous DAPHNE runs. The combination of B and C gives $\eta = 8.2$;

- $P = \langle P_T \rangle \langle P_\gamma \rangle = 0.30$;

- $\epsilon_{det} \simeq 90\%$ is conservatively assumed for the total inclusive photoabsorption cross section;

- $\epsilon_{det} \simeq 20\%$ is assumed for the $n\pi^0$ case; this comes from the combination of the CB neutron efficiency (25%) and the π^0 reconstruction efficiency (80%).

For the total inclusive photoabsorption cross section we aim at a bin size of 20 MeV in photon energy and at a statistical precision of $\delta E_{stat} = 0.01$, which corresponds to an absolute uncertainty $\delta\Delta\sigma = \pm 5\mu$b for a cross section difference $\Delta\sigma = 50\mu$b. The required time to reach this goal in the energy range 800-1450 MeV ($\langle\sigma_{unpol}\rangle \simeq 150\mu$b) is about 100 hours. This data taking will be performed in parallel with the partial channel measurement.

For the $n\pi^0$ process, we aim at a bin size of 20 MeV in photon energy and at 10 bins in the angular distribution with a statistical precision of $\delta E_{stat} = 0.05$, which corresponds to an absolute uncertainty $\delta\Delta\sigma = \pm 0.2\mu$b for a differential cross section difference $\Delta d\sigma/d\Omega = 1.5\mu/sr$. The required beam time to reach this goal is:

- 500 hours in the energy range 800-1450 MeV ($\langle\sigma_{unpol}\rangle \simeq 1.5\mu$b$/sr$)

- 300 hours in the energy range 400-800 MeV ($\langle\sigma_{unpol}\rangle \simeq 2.5\mu$b$/sr$)

- 200 hours in the energy range 150-400 MeV ($\langle\sigma_{unpol}\rangle \simeq 4.0\mu$b$/sr$)

The $n\pi^0\pi^0$ process is expected to have a smaller cross section, especially for photon energies below 1 GeV. In this case the energy bin size will be increased to $\Delta E_\gamma = \pm 20$ MeV, in order to reach similar values for δE_{stat} as before.

Based on the experience with the previous GDH experiment, additional 200 hours will be required for in-beam set-up and tests, target polarisation, photon flux and Møller measurements. Data with a liquid deuterium target will also be needed for unpolarised cross section data, but these can be measured in conjunction with other experiments.

To summarize, a total beam time of:

1200 hours

is then requested for the asymmetry measurement of the total photoabsorption and the partial reaction channels on the polarised deuteron.

6.2 ^{3}He target

The parameters entering the count rate estimate are:

- Incoming electron beam energy: $E_0 = 450$, 855 and 1500 MeV;

- Tagged photon energy range: upper half of the photon energy range;

- Photon flux $I_\gamma = 2.5 \cdot 10^6/(sec \cdot 20$ MeV); this corresponds to the maximum estimated photon flux value allowed by the tagger focal plane detectors.

- polarised target nucleon density ($d = 1$)is $f \cdot N_T = 3 \cdot 10^{21}$ (cm^{-2}) for a 20 cm long target at 6 bar;

- the target dilution factor amounts to $f = 1/3 = 0.3$, due to ^{3}He protons. This gives $B = 2$.

- the background due to the target cell materials is $C = 12$, as estimated in sect. 4.4. The combination of B and C gives $\eta = 15$;

- $P = \langle P_T\rangle\langle P_\gamma\rangle = 0.33$;

- $\epsilon_{det} \simeq 90$ is conservatively assumed for the total inclusive photoabsorption cross section;

- $\epsilon_{det} \simeq 80\%$ is assumed for the π^0 case; this comes from the π^0 reconstruction efficiency (80%).

For the total inclusive photoabsorption cross section we aim at a bin size of 20 MeV in photon energy and at a statistical precision of $\delta E_{stat} = 0.01$, which corresponds to an absolute uncertainty $\delta\Delta\sigma = \pm 5\mu$b for a cross section difference $\Delta\sigma = 50\mu$b. The required time to reach this goal is

- 400 hours in the energy range 800-1400 MeV ($\langle\sigma_{unpol}\rangle \simeq 150\mu$b)

- 300 hours in the energy range 400-800 MeV ($\langle\sigma_{unpol}\rangle \simeq 200\mu$b)

- 200 hours in the energy range 150-400 MeV ($\langle\sigma_{unpol}\rangle \simeq 300\mu$b) This last data taking will be performed in parallel with the measurement of the $\pi^0 X$ partial channel

For the $\pi^0 X$ process, we aim at a bin size of 20 MeV in photon energy and at 10 bins in the angular distribution with a statistical precision of $\delta E_{stat} = 0.07$, which corresponds to an absolute uncertainty $\delta\Delta\sigma = \pm 0.3\mu$b for a differential cross section difference $\Delta d\sigma/d\Omega = 4\mu/sr$. The required beam time to reach this goal is 400 hours.

Based on the experience with the previous A1 and GDH experiments, additional 200 hours will be required for in-beam set-up and tests, target polarisation, photon flux and Møller measurements. To summarize, a total beam time of:

1300 hours

is then requested for the asymmetry measurement of the total photoabsorption and the $\pi^0 X$ partial reaction channels on the polarised ^{3}He .

References

[1] R. M. Woloshyn, Nucl. Phys. **A 496**, 749 (1989).

[2] S.B. Gerasimov, Sov. J. Nucl. Phys. **2**, 430 (1966).

[3] S.D. Drell and A.C. Hearn, Phys. Rev. Lett. **16**, 908 (1966).

[4] R.A. Arndt *et al.*, Phys. Rev. C **66**, 055213 (2002).

[5] D.Drechsel *et al.*, Phys. Rev. D **63**, 114010 (2001).

[6] A. Fix and H. Arenhövel,Eur. Phys. J. A **25**, 115 (2005).

[7] S. Sumowigado and T. Mart, Phys. Rev. C **60**, 028201 (1999).

[8] Q. Zhao, J.S. Al-Khalili and C. Bennhold, Phys. Rev. C **65**, 032201 (2002)

[9] N. Bianchi and E. Thomas, Phys. Lett. **B 450**, 439 (1999).

[10] J. Ahrens *et al.*, Phys. Rev. Lett. **84**, 5950 (2000).

[11] J. Ahrens *et al.*, Phys. Rev. Lett. **87**, 022003 (2001).

[12] H. Dutz *et al.*, Phys. Rev. Lett. **91**, 192001 (2003).

[13] H. Dutz *et al.*, Phys. Rev. Lett. **93**, 032003 (2004).

[14] D. Drechsel and T.W. Walcher, Rev. Mod. Phys. **80**, 731 (2008).

[15] S. Simula *et al.*, Phys. Rev. D **65**, 034017 (2002).

[16] O.A. Rondon, Phys. Rev. C **60**, 035201 (1999).

[17] J. Ahrens *et al.*, Phys. Rev. Lett. **88**, 232002 (2002).

[18] Review of Particle Physics, Phys. Lett. **B 667**, 1 (2008)

[19] J. Ahrens *et al.*, Phys. Lett. **B 551**, 49 (2003).

[20] J. Ahrens *et al.*, Phys. Lett. **B 624**, 173 (2005).

[21] J. Ahrens *et al.*, Eur. Phys. J. A **34**, 11 (2007).

[22] A.V. Anisovich *et al.*, Eur. Phys. J. A **24**, 111 (2005).

[23] J. Ahrens *et al.*, Phys. Lett. **B 672**, 328 (2009).

[24] H. Weller *et al.*, Prog. Part. Nucl. Phys. **62**, 257 (2009).

[25] H. Dutz *et al.*, Phys. Rev. Lett. **94**, 162001 (2005).

[26] B. Krusche *et al.*, Eur. Phys. J. A **17**, 241 (2003).

[27] H.Arenhövel *et al.*, Phys. Rev. Lett. **93**, 202301 (2004).

[28] C. Ciofi degli Atti and S. Scopetta, Phys. Lett. **B 404**, 223 (1997).

[29] M.MacCormick *et al.*, Phys. Rev. C **53**, 41 (1996).

[30] A. Fix, private communication.

[31] A.Deltuva *et al.*, Phys. Rev. C **69**, 034004 (2004).

[32] J.Golak *et al.*, Phys. Rev. C **72**, 044002 (2005).

[33] D. Rohe, Ph.D. thesis, University of Mainz (1998).

[34] J. Bermuth *et al.*, Phys. Lett. **B** 564 (2003) 199.

[35] F. Colegrove, L. Schearer, G. Walters, Phys. Rev. 132 (6) (1963) 2561.

[36] P. Nacher, M. Leduc, J. Physique 46 (1985) 2057.

[37] J. Schmiedeskamp, Ph.D. thesis, University of Mainz (2005).

[38] E. Otten, Europhysics News 35 (2004) 16.

[39] M. Wolf, Ph.D. thesis, University of Mainz (2004).

[40] S. Schlimme, Ph.D. thesis, University of Mainz (in preparation).

[41] J. Krimmer *et al.* in preparation.

[42] L. Schearer, G. Walters, Phys. Rev. **A** 139 (5) (1965) 1398.

[43] N. Newbury, A. Barton, G. Cates, W. Happer, H. Middleton, Phys. Rev. **A** 48 (6) (1993) 4411.

[44] P. Aguar-Bartolome, Diploma thesis, University of Mainz (2005).

[45] E. Wilms, M. Ebert, W. Heil, R. Surkau, Nucl. Instr. Methods **A** 401 (1996) 491.

[46] B. Lannoy, Ph.D. thesis, University of Gent, 2000.

[47] D. Ryckbosch, private communication.

[48] A. Zabrodin *et al.*, Phys. Rev. C **55**, R1617 (1997).

[49] J. Weiss *et al.*, Eur. Phys. J. A **16**, 275 (2003).

[50] T.A Armstrong *et al.*, Phys. Rev. D **5**, 1640 (1972).

[51] O. Bartalini *et al.*, Phys. Atom. Nucl. **71**, 75 (2008).

A Experimental apparatus

A.1 Photon Beam

The A2 photon beam is derived from the production of Bremsstrahlung photons during the passage of the MAMI electron beam through a thin radiator. The resulting photons can be circularly polarised, with the application of a polarised electron beam, or linearly polarised, in the case of a crystalline radiator. The degree of polarisation achieved is dependent on the energy of the incident photon beam (E_0) and the energy range of interest, but currently peaks at $\sim$75% for linear polarisation (Fig. 14) and $\sim$85% for circular polarisation (Fig. 15). The maximum degree of linear polarisation should be further improved by 5 to 10% by the end of 2009 when the collimation and beam monitoring systems will be optimised for MAMI-C during the installation of the Frozen Spin Target. The Glasgow Photon Tagger (Fig 16) provides energy tagging of the photons by detecting the post-radiating electrons and can determine the photon energy with a resolution of 2 to 4 MeV depending on the incident beam energy, with a single-counter time resolution $\sigma_t = 0.117$ ns [2]. Each counter can operate reliably to a rate of $\sim$1 MHz, giving a photon flux of $2.5 \cdot 10^5$ photons per MeV. Photons can be tagged in the momentum range from 4.7 to 93.0% of E_0.
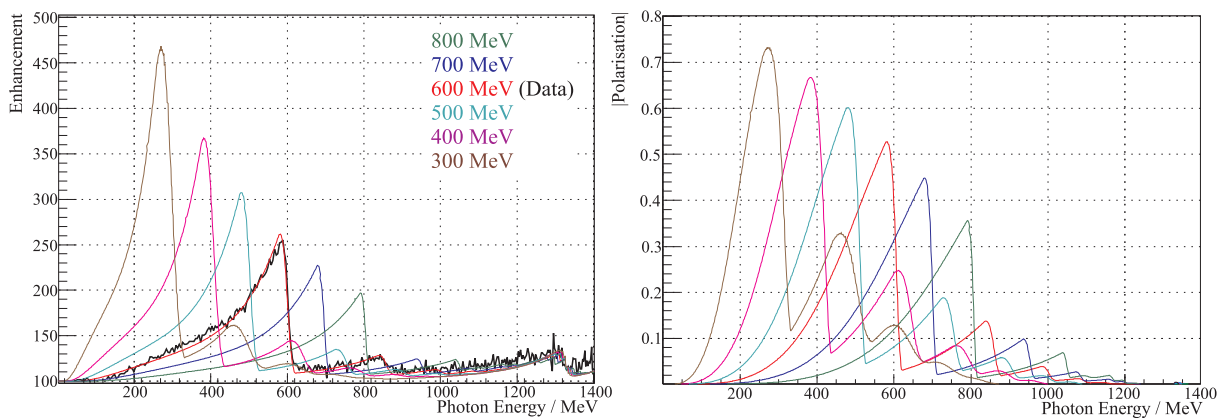

Figure 14: Linear polarisation available with the current collimation system for a variety of crystal orientations. The thin black lines are data obtained during recent MAMI-C runs.

To augment the standard focal plane detector system and make use of the Tagger's intrinsic energy resolution of 0.4 MeV (FWHM), there exists a scintillating fibre detector ('Tagger Microscope') that can improve the energy resolution by a factor of about 6 for a $\sim$100 MeV wide region of the focal plane (dependent on its position) [4].

A.2 Frozen-Spin Target

Polarisation experiments using high density solid-state targets in combination with tagged photon beams can reach the highest luminosities. For the double polarisation measurements planned with the Crystal Ball detector on polarised protons and deuterons a specially designed, large horizontal ^{3}He/^{4}He dilution refrigerator was built in cooperation with the Joint Institute for Nuclear Research (JINR) Dubna (see Figure 17). It has minimum limitations for the particle detection and fits into the central core of the inner Particle Identification Detector (PID2). This was achieved by using the frozen spin technique with the new concept of placing a thin superconducting holding coil inside the polarisation refrigerator. Longitudinal and transverse polarisations will be possible.

Highest nucleon polarisation in solid-state target materials is obtained by a microwave pumping
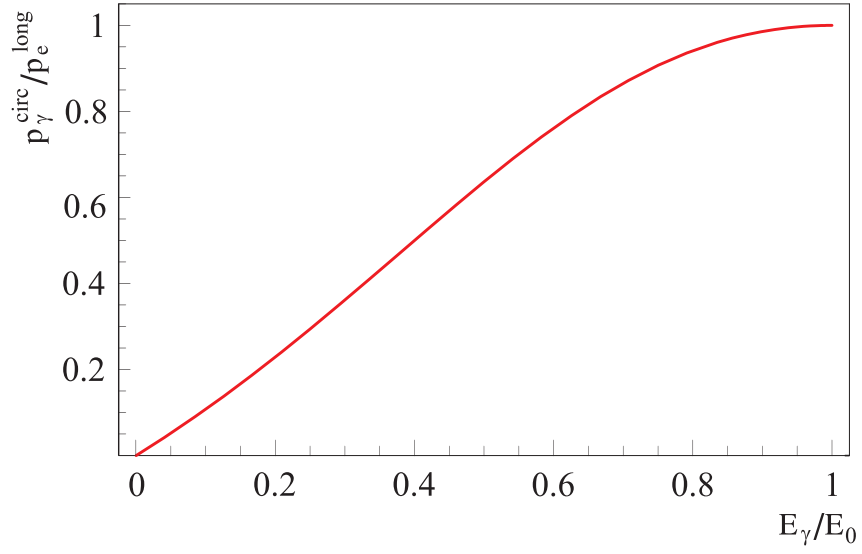
Figure 15: Helicity transfer from the electron to the photon beam as function of the energy transfer. The MAMI beam polarisation is $P_e \approx 85\%$.
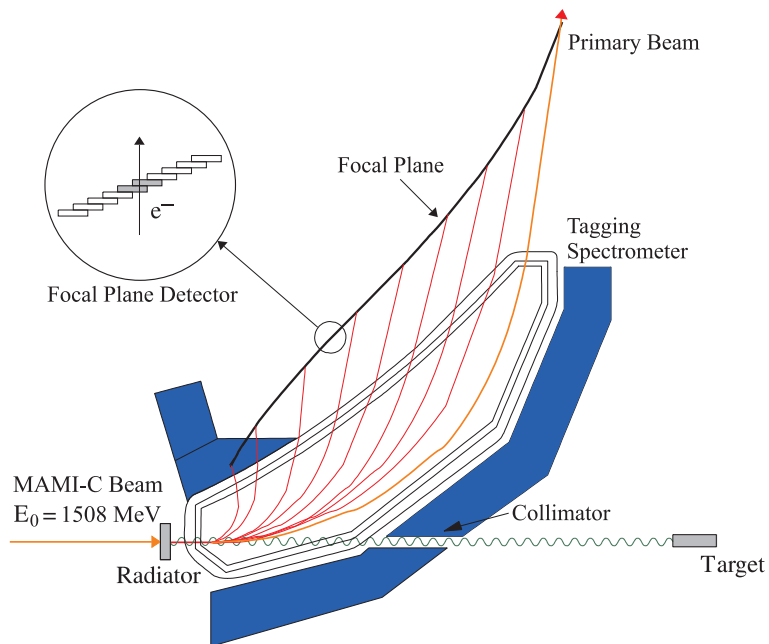

Figure 16: The Glasgow photon tagging spectrometer.

Figure 17: The new dilution refrigerator for the Crystal Ball Frozen Spin Target.

process, known as 'Dynamic Nucleon Polarisation' (DNP). This process is applicable to any nucleus with spin and has already been used in different experiments with polarised proton and deuteron targets. The geometric configuration of the target is the same for the polarised proton and neutron setup. However, since the polarisation measurement of the deuteron is more delicate due to the small size of the polarisation signals, the modification of some basic components is needed. The reason for this is twofold: firstly the magnetic moment of the deuteron is smaller than that of the proton and, in addition, the interaction of the deuteron quadrupole moment with the electric field gradient in the sample broadens the deuteron polarisation signal. An accuracy $\delta P_p / P_p$ of 2 to 3% for the protons and $\delta P_D / P_D$ of 4 to 5% for the deuterons is expected in the polarisation measurement. It has also to be taken into account that the measured deuteron polarisation P_D is not equal to the neutron polarisation P_n. Assuming a 6 % admixture of the D-state of the deuteron, a calculation based on the Clebsch-Gordon coefficients leads to $P_n = 0.91 \, P_D$. Several polarised proton and deuteron materials are available such as alcohols and deuterated alcohols (e.g. butanol C_4H_9OH), NH_3, ND_3 or ^6LiD. The most important criteria in the choice of material suitable for particle physics experiments are the degree of polarisation P and the ratio k of free polarisable nucleons to the total number of nucleons. Further requirements on polarised target materials are a short polarisation build-up time and a simple, reproducible target preparation. The polarisation resistance against radiation damage is not an issue for experiments with a low intensity tagged photon beam ($\dot{N}_\gamma \approx 5 \cdot 10^7 \text{ s}^{-1}$) as will be used here. However, the limitations of a reduced relaxation time due to overheating of the target beads (Kapitza resistance) will have to be investigated.

Taking all properties together, butanol and deuterated butanol are the best material for this experiment. For protons we expect a maximum polarisation of $P_p = 90\%$ and an average polarisation of $P_p = 70\%$ in the frozen spin mode. Recently, a deuteron polarisation $P_D = 80\%$

was obtained with Trityl doped butanol targets at 2.5 T magnetic field in a ^{3}He/^{4}He dilution refrigerator. At a 0.4 T holding field an average neutron polarisation P_n (see above) of 50 % will be obtained. The filling factor for the ~2 mm diameter butanol spheres into the 2 cm long, 2 cm diameter target container will be around 60%. The experience from the GDH runs in 1998 [5] shows that, with a total tagged photon flux of $5 \cdot 10^7$, relaxation times of about 200 hours can be expected. The polarisation has to be refreshed by microwave pumping every two days. In conclusion, we estimate that we will achieve the following target parameters:

- Maximum total tagged photon flux in the energy range of 4.7 to 93% of E_0: $\dot{N}_\gamma \approx 5 \cdot 10^7 \mathrm{s}^{-1}$, with relaxation time of 200 hours.

- Target proton density in 2 cm cell: $N_T \approx 9.1 \cdot 10^{22} \mathrm{cm}^{-2}$ (including dilution and filling factors)

- Average proton polarisation $P_p = 70\%$

- Target deuteron density in 2cm cell: $N_T \approx 9.4 \cdot 10^{22} \mathrm{cm}^{-2}$ (including dilution and filling factors)

- Average neutron polarisation $P_n = 50\%$

A.3 Crystal Ball Detector System

The central detector system consists of the Crystal Ball calorimeter combined with a barrel of scintillation counters for particle identification and two coaxial multiwire proportional counters for charged particle tracking. This central system provides position, energy and timing information for both charged and neutral particles in the region between 21° and 159° in the polar angle (θ) and over almost the full azimuthal (ϕ) range. At forward angles, less than 21°, reaction products are detected in the TAPS forward wall. The full, almost hermetic, detector system is shown schematically in Fig. 18 and the measured two-photon invariant mass spectrum is shown in Fig. 19.

The Crystal Ball detector (CB) is a highly segmented 672-element NaI(Tl), self triggering photon spectrometer constructed at SLAC in the 1970's. Each element is a truncated triangular pyramid, 41 cm (15.7 radiation lengths) long. The Crystal Ball has an energy resolution of $\Delta E/E = 0.020 \cdot E[GeV]^{0.36}$, angular resolutions of $\sigma_\theta = 2 \ldots 3°$ and $\sigma_\phi = \sigma_\theta / \sin\theta$ for electromagnetic showers [1]. The readout electronics for the Crystal Ball were completely renewed in 2003, and it now is fully equipped with SADCs which allow for the full sampling of pulse-shape element by element. In normal operation, the onboard summing capacity of these ADCs is used to enable dynamic pedestal subtraction and the provision of pedestal, signal and tail values for each element event-by-event. Each CB element is also newly equipped with multi-hit CATCH TDCs. The readout of the CB is effected in such a way as to allow for flexible triggering algorithms. There is an analogue sum of all ADCs, allowing for a total energy trigger, and also an OR of groups of sixteen crystals to allow for a hit-multiplicity second-level trigger - ideal for use when searching for high multiplicity final states.

In order to distinguish between neutral and charged particles species detected by the Crystal Ball, the system is equipped with PID2, a barrel detector of twenty-four 50 mm long, 4 mm thick scintillators, arranged so that each PID2 scintillator subtends an angle of 15° in ϕ. By matching a hit in the PID2 with a corresponding hit in the CB, it is possible to use the locus of the $\Delta E, E$ combination to identify the particle species (Fig. 20). This is primarily used for the separation of charged pions, electrons and protons. The PID2 covers from 15° to 159° in θ.

The excellent CB position resolution for photons stems from the fact that a given photon triggers several crystals and the energy-weighted mean of their positions locates the photon position to better than the crystal pitch. For charged particles which deposit their energy over only one or
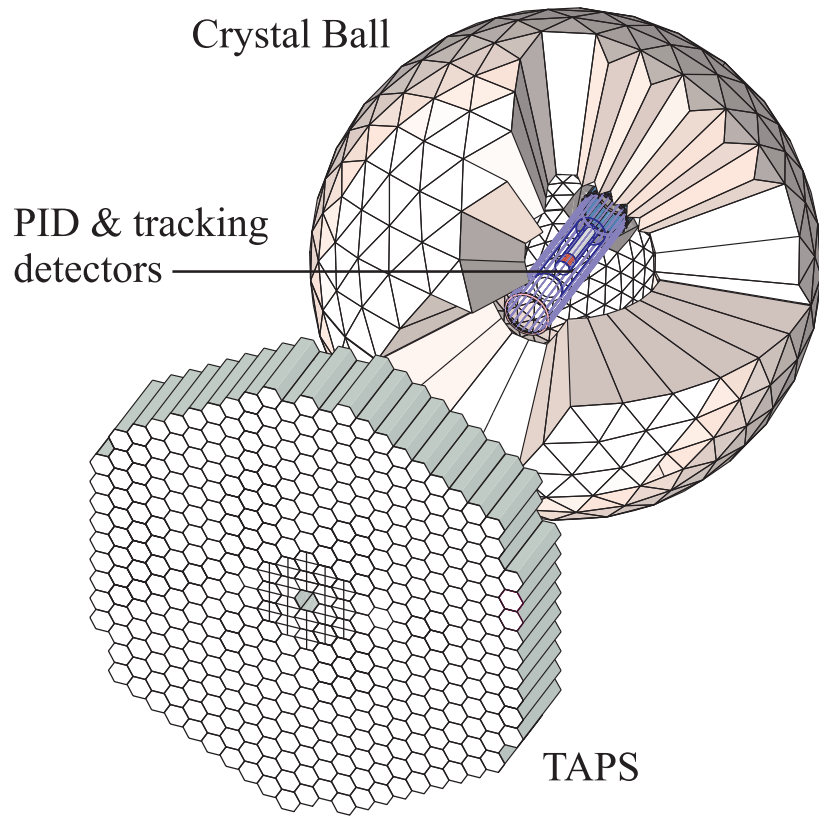
Figure 18: The A2 detector setup: The Crystal Ball calorimeter, with cut-away section showing the inner detectors, and the TAPS forward wall.
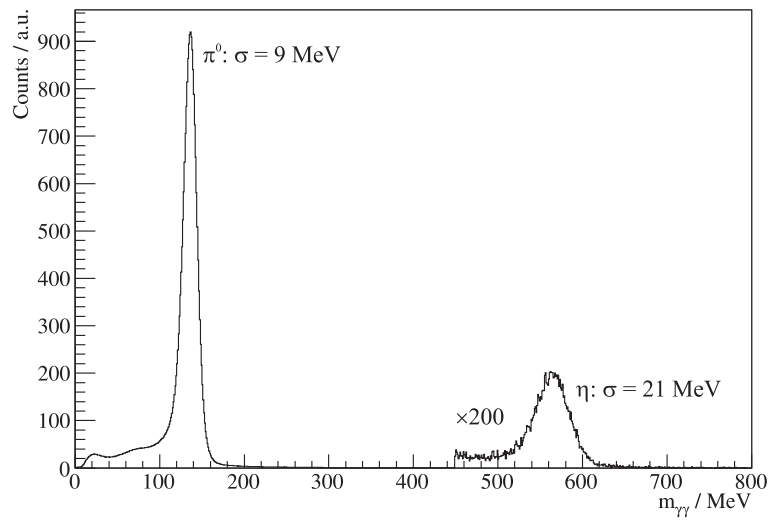

Figure 19: Two photon invariant mass spectrum for the CB/TAPS detector setup. Both η and π^0 mesons can be clearly seen.
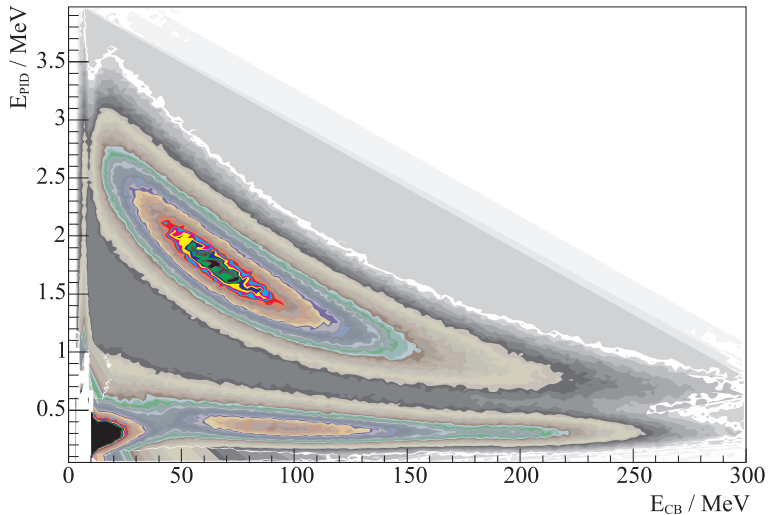
Figure 20: A typical $\Delta E/E$ plot from the Crystal Ball and the PID2 detector. The upper curved region is the proton locus, the lower region contains the pions and the peak towards the origin contains mostly electrons.

two crystals, this is not so precise. Here the tracks of charged particles emitted within the angular and momentum acceptance of the CB detector will be reconstructed from the coordinates of point of intersections of the tracks with two coaxial cylindrical multiwire proportional chambers (MWPCs) with cathode strip readout. These MWPCs are similar to those installed inside the CB during the first round of MAMI-B runs [3]. The most significant difference is that all detector signals are taken at the upstream end of the MWPCs, minimising the material required and facilitating particle detection in the forward polar region.

A mixture of argon (79.5%), ethane (30%) and freon-CF_4 (0.5%) is used as the filling gas. This mixture is a compromise between charge multiplication and localization requirements imposed by the ionizing particle tracks.

Within each chamber both the azimuthal and the longitudinal coordinates of the avalanche will be evaluated from the centroid of the charge distribution induced on the cathode strips. The location of the hit wires(s) will be used to resolve ambiguities which arise from the fact that each pair of inner and outer strip cross each other twice. The expected angular resolution (rms) will be $\sim 2°$ in the polar emission angle θ and $\sim 3°$ in the azimuthal emission angle ϕ.

The MWPCs have been recently installed inside the CB frame and their calibration using both cosmic rays and test beam data is currently underway.

A.4   TAPS Forward Wall

The TAPS forward wall is composed of 384 BaF_2 elements, each 25 cm in length (12 radiation lengths) and hexagonal in cross section, with a diameter of 59 mm. The front of every TAPS element is covered by a 5 mm thick plastic veto scintillator. The single counter time resolution is $\sigma_t = 0.2$ ns, the energy resolution can be described by $\Delta E/E = 0.018 + 0.008/E[GeV]^{0.5}$ [1]. The angular resolution in the polar angle is better than $1°$, and in the azimuthal angle it improves with increasing θ, being always better than $1/R$ radian, where R is the distance in centimeters from the central point of the TAPS wall surface to the point on the surface where the particle trajectory meets the detector. The TAPS readout was custom built for the beginning of the CB@MAMI program and is effected in such a way as to allow particle identification by Pulse Shape Analysis (PSA), Time Of Flight (TOF) and $\Delta E/E$ methods (using the energy deposit in the plastic scintillator to give ΔE). TAPS can also contribute to the CB multiplicity trigger

and is currrently divided into upto six sectors for this purpose. The 2 inner rings of 18 BaF_2 elements have been replaced recently by 72 $PbWO_4$ crystals each 20 cm in length (22 radiation lengths). The higher granularity improves the rate capability as well as the angular resolution. The crystals are operated at room temperature. The energy resolution for photons is similar to BaF_2 under these conditions [6].

References

[1] S. Prakhov et al.: *Measurement of the Slope Parameter α for the $\eta \to 3\pi^0$ decay with the Crystal Ball dectector at the Mainz Microtron (MAMI-C)*, Phys. Rev. **C 79** (2009) 035204

[2] J.C. McGeorge et al.: *Upgrade of the Glasgow photon tagging spectrometer for Mainz MAMI-C*, Eur. Phys. J. **A 37** (2008) 129

[3] G. Audit et al.: *DAPHNE: a large-acceptance tracking detector for the study of photoreactions at intermediate energies*, Nucl. Instr. Meth. **A 301** (1991) 473

[4] A. Reiter et al.: *A microscope for the Glasgow photon tagging spectrometer in Mainz*, Eur. Phys. J. **A 30** (2006) 461

[5] A. Thomas et al.: *The GDH Experiment at MAMI*, Nucl. Phys. **B 79** (1999) 591

[6] R. Novotny *et al.*: *Scintillators for photon detection at medium energies: A comparative study of BaF-2, CeF-3 and PbWO-4*, Nucl. Instrum. Meth. A **486** (2002) 131